Effects of the synchro-betatron coupling induced by dipole-field modulation

Y. Wang,[1] M. Ball,[1] B. Brabson,[1] J. Budnick,[1] D.D. Caussyn,[1] A.W. Chao,[2] J. Collins,[1] V. Derenchuk,[1] S. Dutt,[2] G. East,[1] M. Ellison,[1] D. Friesel,[1] B. Hamilton,[1] H. Huang,[1] W.P. Jones,[1] S.Y. Lee,[1] D. Li,[1] J.Y. Liu,[1] M.G. Minty,[3] K.Y. Ng,[4] X. Pei,[6] A. Riabko,[1] T. Sloan,[1] M. Syphers,[2] L. Teng,[5] Y.T. Yan,[2] and P.L. Zhang[2]

[1] *Indiana University Cyclotron Facility, Indiana University, Bloomington, Indiana 47405*
[2] *The SSC Laboratory, 2550 Beckleymeade Avenue, Dallas, Texas 75237-3946*
[3] *Stanford Linear Accelerator Center, MS26, Box 4349, Stanford, California 94309*
[4] *Fermilab, P.O. Box 500, Batavia, Illinois 60510*
[5] *Argonne National Laboratory, 9700 South Cass Avenue, Argonne, Illinois 60439*
[6] *Brookhaven National Laboratory, Upton, New York 11973*

(Received 13 September 1993)

The synchro-betatron coupling induced by modulating a transverse dipole field at a frequency close to the synchrotron frequency was studied experimentally. The combination of the electron cooling and transverse-field modulation on the synchrotron oscillation is equivalent to a dissipative parametric resonant system. Six-dimensional Poincaré maps were measured at ten-turn intervals. The proton bunch was observed to split longitudinally into two pieces, or beamlets, converging toward attractors of the dissipative system within a rf bucket. Based on our experimental results, the effects of ground vibration on the superconducting supercollider beam and the effects of power-supply ripple on the relativistic heavy-ion collider beam are examined.

PACS number(s): 41.85.−p, 03.20.+i, 05.45.+b, 29.20.Dh

I. INTRODUCTION

The equation of motion for phase oscillations of a particle in a synchrotron is given by [1]

$$\ddot{\phi} + \omega_s^2(\sin\phi - \sin\phi_0) = 0, \tag{1.1}$$

where ϕ is the relative rf phase angle between the orbiting particle and the rf phase, $\omega_s = \omega_0\sqrt{\frac{heV|\eta|}{2\pi\beta^2 E}}$ is the small-amplitude synchrotron angular frequency at $\phi_0 = 0$, ω_0 is the angular revolution frequency, h, V, and ϕ_0 are respectively the harmonic number, the peak rf voltage, and the synchronous phase angle, βc and E are respectively the speed and the energy of the particle, and η is the phase slip factor. Thus particles are executing synchrotron oscillations longitudinally around the synchronous particle.

Transversely, the horizontal and vertical deviations from the closed orbit of a beam particle satisfy Hill's equation [2]:

$$\frac{d^2x}{ds^2} + K_x(s)x = \frac{\Delta B_z}{B\rho}, \quad \frac{d^2z}{ds^2} + K_z(s)z = -\frac{\Delta B_x}{B\rho}. \tag{1.2}$$

Here $K_x(s), K_z(s)$ are focusing functions, $B\rho$ is the magnetic rigidity, s is the longitudinal particle coordinate, and $\Delta B_x, \Delta B_z$ are linear or nonlinear error magnetic fields. In the linear approximation, the solution of the error-free transverse Hill's equation is

$$y = \sqrt{2\beta_y(s)J_y}\cos[\phi_y(s) + \chi_y], \quad \phi_y(s) = \int_0^s \frac{ds}{\beta_y},$$

where y stands for either x or z. Here $\beta_y(s)$ is the betatron amplitude function, J_y is the invariant action, $\phi_y(s)$ is the betatron phase advance, and χ_y is an initial phase angle. The numbers of betatron oscillations in one revolution are called betatron tunes defined as $\nu_y = \frac{1}{2\pi}\oint\frac{ds}{\beta y}$. Thus particles are executing betatron oscillations transversely about the closed orbit of an accelerator.

Coupled motion between the transverse and longitudinal degrees of freedom is called synchro-betatron (SB) coupling. The SB coupling is significant for electron storage rings [3], where the fractional parts of the synchrotron and betatron tunes are of the same order of magnitude. Similarly, the SB coupling can also be important for fast cycling proton synchrotrons, such as the Fermilab Booster, where the synchrotron tune is of the order of 0.1. On the other hand, the fractional part of the betatron and synchrotron tunes differ substantially in proton storage rings, and the coupling between longitudinal and transverse motions is not as important. However low-frequency transverse oscillations may couple to the synchrotron degree of freedom. For the superconducting supercollider (SSC), where the synchrotron frequency varies from 7 Hz at injection energy to 4 Hz at 20 TeV, SB coupling may arise from ground vibration. At the relativistic heavy-ion collider (RHIC), the synchrotron frequency ramps through 60 Hz around 17 GeV/c for heavy-ion beams, and SB coupling may result from power-supply ripple.

The dominant effect of ground vibration or power-supply ripple is a modulation of dipole field. A slow adiabatic dipole modulation gives rise to a closed-orbit mod-

ulation. Provided that the resulting closed-orbit modulation is much smaller than the beamwidth, the adiabatic modulation usually does not limit the performance of colliders or storage rings. Detailed analyses have been reported and compiled [4]. However, performance degradation can arise from nonadiabatic modulations, which occur naturally at resonance conditions, e.g., transverse modulation at the synchrotron frequency. The resulting motion can also be characterized as SB coupling. A detailed study of this issue is therefore needed.

We have recently studied and reported experimental results of SB coupling arising from the dipole-field modulation at frequencies close to the synchrotron frequency [5]. This paper is intended to present our data analysis based on the Hamiltonian formulation and determine the tolerance of the SB coupling due to ground vibration or power-supply ripple. The plan of this paper is as follows. In Sec. II, the experimental method and data analysis will be presented. In Sec. III, the synchrotron motion with phase modulation resulting from the SB coupling is formulated in terms of the Hamiltonian dynamics and the tolerance of the SSC to the ground vibration and the consequences of power-supply ripple for RHIC are discussed. The conclusion is given in Sec. IV.

II. EXPERIMENTAL METHOD AND DATA ANALYSIS

The experimental procedure started with a single bunch of about 5×10^8 protons with kinetic energy of 45 MeV at the Indiana University Cyclotron Facility (IUCF) Cooler synchrotron. The cycle time was 11 s. The injected beam was electron-cooled and was modulated simultaneously by a small dipole. A 23-cm window-frame ferrite dipole magnet [6] was used to produce the transverse dipole-field modulation. The effective length of the dipole was measured to be $\ell = 0.27$ m. The horizontal dispersion function was $D_x \approx 4.0$ m at the modulation dipole location. At the end of 7 s, the beam-centroid displacements were digitized, and recorded from signals of beam position monitors (BPM's). The longitudinal phase coordinate was measured by comparing the time difference between the signal from a BPM sum signal passing through a 1.4-MHz low-pass filter and the signal from the rf clock. A beam position monitor with a low-pass filter (3 kHz) at a high-dispersion location was used to measure the momentum deviation, which is related to the off-momentum closed orbit by $\Delta x_{\rm p} = D_x \frac{\Delta p}{p}$ with $D_x \approx 3.9$ m. A total of 8 channels were used to obtain six-dimensional (6D) phase-space maps with 16 384 points recorded at ten-turn intervals. Details of our data acquisition system have been reported earlier [7, 8].

For this experiment, the harmonic number was $h = 1$, the phase slip factor was $\eta \approx -0.86$, the stable phase angle was $\phi_0 = 0$, and the revolution frequency was $f_0 = \frac{\omega_0}{2\pi} = 1.031\,68$ MHz. The rf voltage was chosen to be 41 V to obtain a synchrotron frequency of $f_s = \frac{\omega_s}{2\pi} = 262$ Hz in order to avoid harmonics of the 60-Hz ripple. The synchrotron tune was $\nu_s = \frac{\omega_s}{\omega_0} = 2.54 \times 10^{-4}$. We chose $\nu_x = 3.828, \nu_z = 4.858$ for this experiment to avoid nonlinear betatron resonances. The corresponding smallest horizontal and vertical betatron sideband frequencies were 177 and 146 kHz, respectively.

With a horizontal dipole (vertical field) modulation at location s_0, the horizontal closed-orbit deviation $x_d(t)$ becomes [2]

$$x_d(t) = \frac{\sqrt{\beta_x(s)\beta_x(s_0)}}{2\sin\pi\nu_x}\theta(t)\cos[\pi\nu_x - |\phi_x(s) - \phi_x(s_0)|],$$

where $\theta(t) = \hat{\theta}\sin(\omega_m t + \chi_0)$ with $\hat{\theta} = \frac{\hat{B}_m \ell}{B\rho}$ and $\hat{B}_m$ as the peak modulation dipole field. Furthermore, if the dispersion function at the modulating dipole location is not zero, the path length is also modulated. The change in the circumference is given by

$$\Delta C = D_x\theta(t) = D_x\hat{\theta}\sin(\omega_m t + \chi_0), \tag{2.1}$$

where D_x is the dispersion function at the modulation dipole location. The corresponding rf phase difference becomes $\Delta\phi = 2\pi h\frac{\Delta C}{C}$, where $C = 86.82$ m is the circumference of the IUCF Cooler Ring. In our experiment, the maximum rf phase shift per turn $\hat{\Delta\phi}$ was $0.78\times10^{-5}\hat{B}_m$ [gauss] radians.

The longitudinal phase-space coordinates $(\phi, \frac{\Delta p}{p})$ at the nth and the $(n+1)$th revolutions are transformed according to the following mapping equations:

$$\phi_{n+1} = \phi_n + 2\pi h\eta\left(\frac{\Delta p}{p}\right)_n + \Delta\phi, \tag{2.2}$$

$$\left(\frac{\Delta p}{p}\right)_{n+1} = \left(\frac{\Delta p}{p}\right)_n + \frac{eV}{\beta^2 E}\sin\phi_{n+1} - \lambda\left(\frac{\Delta p}{p}\right)_n, \tag{2.3}$$

where the fractional momentum deviation of particles $(\frac{\Delta p}{p})$ is the conjugate variable to the synchrotron phase angle ϕ, and λ is the phase-space damping parameter related to electron cooling. Thus the synchrotron equation of motion, in the presence of transverse modulation, becomes

$$\frac{d^2\phi}{dt^2} + 2\alpha\frac{d\phi}{dt} + \omega_s^2\sin\phi = \omega_m\omega_s a\cos\omega_m t + 2\alpha\omega_s a\sin\omega_m t, \tag{2.4}$$

where the damping coefficient is $\alpha = \frac{\omega_0}{4\pi}\lambda$. With an electron current of 0.75 A, the damping time for the 45 MeV protons was measured to be about 0.33 ± 0.1 s or $\alpha = 3 \pm 1\ \mathrm{s}^{-1}$ [8], which was indeed small compared with $\omega_s = 1646\ \mathrm{s}^{-1}$.

Because the synchrotron frequency is much smaller than the revolution frequency in proton storage rings, the phase errors of each turn accumulate. The equivalent phase modulation amplitude is enhanced by the factor $\frac{\omega_0}{2\pi\omega_s}$, i.e., the effective phase modulation amplitude parameter a is given by

$$a = \frac{h\omega_0 D_x\hat{\theta}}{\omega_s C} = \frac{\omega_0}{2\pi\omega_s}\hat{\Delta\phi}. \tag{2.5}$$

Although the cooling was weak, the transient solution of Eq. (2.4) has damped out by the time of measurement. We therefore measured the steady-state solution, in con-

trast to our earlier experiment where the transient solutions were measured [8]. Let the steady-state solution of the nonlinear parametric dissipative resonant system, Eq. (2.4), be given by

$$\phi \approx g \sin(\omega_m t - \chi), \tag{2.6}$$

where we have used the approximation of a single harmonic [9]. Expanding the term $\sin\phi$ in Eq. (2.4) up to the first harmonic, we obtain the equation for the modulation amplitude g as

$$[-\omega_m^2 g + 2\omega_s^2 J_1(g)]^2 + [2\alpha\omega_m g]^2 = [\omega_m\omega_s a]^2 + [2\alpha\omega_s a]^2, \tag{2.7}$$

with the phase χ given by

$$\chi = \arctan\left[\frac{g\omega_m(\omega_m^2 + 4\alpha^2) - 2\omega_s^2\omega_m J_1(g)}{4\alpha\omega_s^2 J_1(g)}\right], \tag{2.8}$$

where J_1 is the Bessel function [10] of order 1. Steady-state solutions of Eq. (2.7) are attractors for this dissipative system. The existence of a unique phase factor χ for solutions of the dissipative parametric resonant equation implies that the attractor is a single phase-space point rotating at the modulation frequency ω_m.

There are three solutions to Eq. (2.7) when the modulation frequency is below the critical bifurcation frequency, ω_c, given by the condition

$$\left.\frac{\partial\omega_m}{\partial g}\right|_{\omega_m=\omega_c} = 0.$$

A stable solution with a large phase amplitude g_a and the phase factor $\chi_a \approx \frac{\pi}{2}$ is called the outer attractor solution, and a stable solution at a smaller phase amplitude g_b with $\chi_b \approx -\frac{\pi}{2}$ called the inner attractor solution. A third solution g_c with $\chi_c \approx -\frac{\pi}{2}$ corresponds to the unstable (hyperbolic) solution. When the damping parameter α is small, these two stable solutions are almost opposite to each other in the synchrotron phase space. They rotate about the origin at the modulation frequency [see Eq. (2.6)]. When the damping parameter α is increased, the stable solution (g_a, χ_a) and the unstable solution (g_c, χ_c) approach each other. They collide and disappear for a large damping parameter. Figure 1 shows the phase amplitude g as a function of f_m, calculated from Eq. (2.7) for $\hat{B}_m = 2$ G with $\alpha = 2.5\ \mathrm{s}^{-1}$ and $10\ \mathrm{s}^{-1}$. Note that the outer attractor solution disappears at a large damping parameter. When the modulation frequency is larger than the bifurcation frequency, only the outer attractor solution exists.

When the modulation frequency is far away from the bifurcation frequency, the response amplitude for the inner attractor at $\omega_m \ll \omega_c$ or the outer attractor at $\omega_m \gg \omega_c$ can be approximated by the solution of the linearized Eq. (2.7), i.e.,

$$g = \sqrt{\frac{(\omega_m\omega_s)^2 + (2\alpha\omega_s)^2}{(\omega_s^2 - \omega_m^2)^2 + (2\alpha\omega_m)^2}}\ a. \tag{2.9}$$

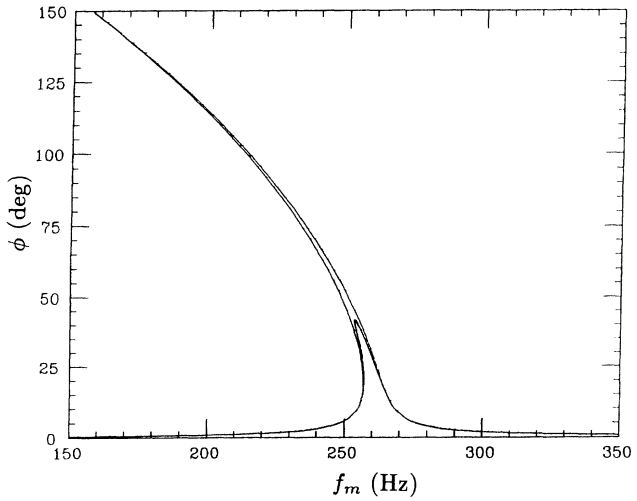

FIG. 1. The attractor solutions of Eq. (2.7) [with the ordinate $\phi = g$] for $\alpha = 2.5\ \mathrm{s}^{-1}$ and $10\ \mathrm{s}^{-1}$ at $\hat{B}_m = 2$ G. Note here that when the damping rate α is larger than $10\ \mathrm{s}^{-1}$, the outer attractor disappears at modulation frequencies below 253 Hz.

A. Observation of attractors

The injected beam from the IUCF K200 azimuthal varying field cyclotron is uniformly distributed in the synchrotron phase space within a momentum spread of about $\frac{\Delta p}{p} \approx \pm 3 \times 10^{-4}$, therefore all attractors can be populated. The phase coordinates of these attractors could be measured by observing the longitudinal beam profile from BPM sum signals on an oscilloscope. Figure 2 shows the longitudinal beam profile accumulated through many synchrotron periods with the modulation field $\hat{B}_m = 4$ G for the modulation frequencies of 210, 220, 230 240, 250, and 260 Hz. The rf wave form was also shown for reference.

It was puzzling, at first, that the longitudinal profile exhibited gaps in the time domain seemingly as if there was no synchrotron motion for the beam bunch located at a relatively large phase amplitude. However, using a fast sampling digital oscilloscope (HP54510A) for a single trace, we found that the beam profile was not made of particles distributed in a ring of large synchrotron amplitude, but rather was composed of two beamlets. Both of these two beamlets rotated in the synchrotron phase space at the modulating frequency, as measured from the fast Fourier transform (FFT) of the phase signal. If the equilibrium distribution of the beamlet was elongated then the sum signal, which measured the peak current of the beam, would show a large signal at both extremes of its phase coordinate, where the peak current was large. When the beamlet rotated to the central position in the phase coordinate, the beam profile became flat with a smaller peak current. Therefore the profile observed with the oscilloscope offered an opportunity to study the equilibrium distribution of charges in these attractors.

Assuming an equilibrium elliptical beamlet profile with Gaussian distribution, the distribution function (current

density) becomes (see Sec. III B)

$$\rho(\phi,t)=\frac{\rho_1}{\sqrt{2\pi}\sigma_1}e^{-\frac{[\phi-\phi_1(t)]^2}{2\sigma_1^2}}+\frac{\rho_2}{\sqrt{2\pi}\sigma_2}e^{-\frac{[\phi-\phi_2(t)]^2}{2\sigma_2^2}}, \tag{2.10}$$

where ρ_1 and ρ_2 depict the relative population of these two beamlets with $\rho_1+\rho_2=1$. Since each particle in these two beamlets rotates in the phase space at the modulating frequency ω_m, the parameters $\phi_{1,2}$ and $\sigma_{1,2}$ are given by

$$\phi_1(t)=g_a\sin(\omega_m t-\chi_a),\quad \phi_2(t)=g_b\sin(\omega_m t-\chi_b),$$

and

$$\sigma_1^2=\sigma_{10}^2(1+r_1\sin^2\omega_m t),\quad \sigma_2^2=\sigma_{20}^2(1+r_2\sin^2\omega_m t).$$

Here $g_{a,b}$ and $\chi_{a,b}$ are the amplitudes and phases of these two beamlets obtained from solving Eqs. (2.7) and (2.8). Since the profile observed on the oscilloscope was accumulated through many synchrotron periods, it would not depend on the parameters $\chi_{a,b}$, i.e., these profiles were not sensitive to the relative positions of these two beamlets. The eccentricity parameters $r_{1,2}$ signify the aspect ratio of these two beamlets, and σ_{10},σ_{20} represent the average rms bunch length. For example, the aspect ratio, given by $1:1+r_1$ of the outer beamlet at the modulation frequency of 220 Hz was found to be about 1:3 from the profile of Fig. 2. This means that the peak current for the outer beamlet was reduced by a factor of 3 when the beamlet rotated to the center of the phase coordinate. The relative population of these two beamlets was about 75% for the inner and 25% for the outer, obtained from fitting the data. As the modulating frequency increased toward the synchrotron frequency, the phase amplitude of the outer beamlet became smaller and its population increased. When the modulating frequency was higher than a critical frequency, ω_c, the center peak disappeared (see the 260-Hz data of Fig. 2).

Figure 3 shows the phase amplitude of the outer beamlet measured with the oscilloscope (squares) and the phase amplitude obtained from the phase detector (diamonds). Since the phase detector was not intended for use with more than one beam bunch present, it appeared that the phase detector measured the centroid of these two beamlets. Only when one beamlet dominated the charge distribution was the phase detector able to measure the phase properly. In the bottom part of Fig. 3 the phase response data from a square-wave modulation were shown to compare with the attractor solutions. Since the square wave can be expanded in Fourier series, $\frac{4}{\pi}\hat{B}_{sq}\sin\omega_{sq}t+\frac{4}{3\pi}\hat{B}_{sq}\sin 3\omega_{sq}t+\cdots$, a peak in the response was expected and observed at a modulation frequency of 87.3 Hz.

To verify that the synchro-betatron coupling observed was caused by dipole modulation in a region with disper-

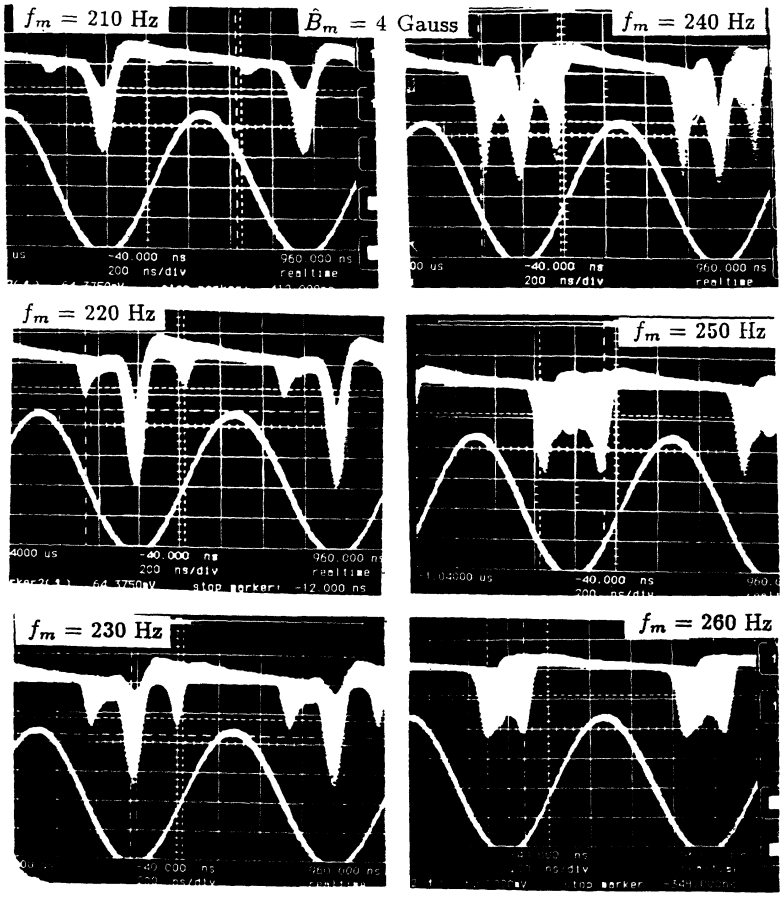

FIG. 2. The oscilloscope traces of accumulated BPM sum signals showed the splitting of beam bunch into beamlets below the bifurcation frequency. The modulation amplitude was $\hat{B}_m$ = 4 G. The sine waves in this figure were the rf wave form.

sion as described in Eq. (2.1), we installed the modulation dipole at a low-dispersion location and repeated the measurement of the beam response for modulation frequency around the synchrotron frequency. Our experimental results confirmed that the effective phase modulation amplitude parameter a was greatly reduced.

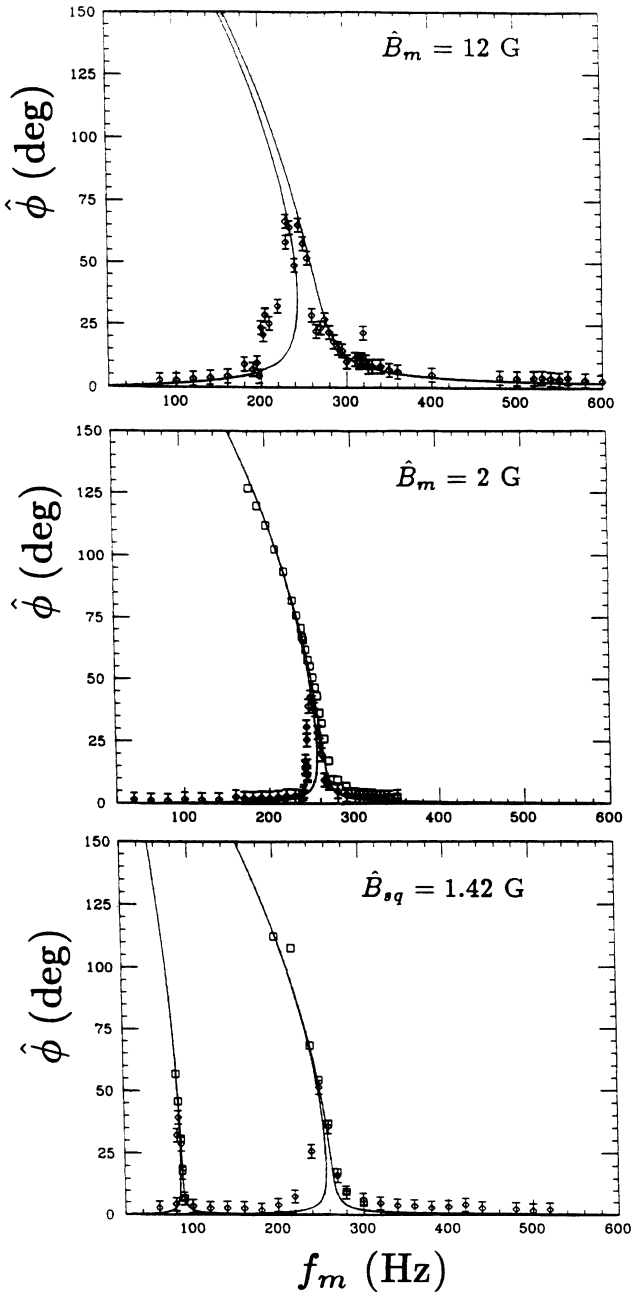

FIG. 3. The phase amplitude of outer beamlet measured from the oscilloscope trace (square) and from the digitizing system (diamond) are plotted as functions of modulation frequency for the sinusoidal wave at $\hat{B}_m$ = 12 G (top), $\hat{B}_m$ = 2 G (middle) and the square wave at $\hat{B}_{sq}$ = 1.42 G (bottom) respectively. For the square-wave modulation, large-amplitude response was expected and observed at $3\omega_m = \omega_s$. Here $\hat{\phi} = g$.

B. The hysteretic phenomena of attractors

The phase amplitudes of attractors shown in Fig. 3 also exhibited hysteresis phenomena. When the modulation frequency, which was started initially above the bifurcation frequency, was ramped downward, the phase amplitude of the synchrotron oscillations would increase along the outer attractor solution. When it reached a frequency far below the bifurcation frequency, the phase amplitude jumped from the outer attractor to the inner attractor solution. On the other hand, if the modulation frequency, when originated from a value far below the bifurcation frequency, was ramped up toward the bifurcation frequency, the amplitude of the phase oscillations followed the inner attractor solution. At a modulation frequency near the bifurcation frequency, the amplitude of the synchrotron oscillations jumped from the inner to the outer attractor solution.

The hysteresis depended on the beam current and the modulation amplitude a. Since a large damping parameter could destroy the outer attractor shown in Fig. 1, the hysteresis would depend also on the dissipative force. The observed phase amplitudes were found to agree well with the solutions of Eq. (2.7). Similar hysteretic phenomena have also been observed in electron-positron colliders related to the beam-beam interactions [11]. At a large beam-beam tune shift, the vertical beam size exhibited a flip-flop effect with respect to the relative horizontal displacement of the two colliding beams. The amplitudes of the coherent π-mode oscillations also showed hysteretic phenomena [11].

C. The effect of 60-Hz ripple

During the experiment, the power supply to the modulation dipole had inadvertently picked up 60-Hz ripple from the transmission line. Thus the actual modulation dipole field was given by

$$\begin{aligned} B_m &= [\hat{B}_m \sin\omega_m t]\ (1 + R\cos\omega_{60} t) \\ &\approx \hat{B}_m \sin\omega_m t + \frac{1}{2}\hat{B}_m R(\sin[\omega_m + \omega_{60}]t \\ &\quad + \sin[\omega_m - \omega_{60}]t), \end{aligned} \tag{2.11}$$

where R represented the amplitude of the 60-Hz ripple. This effect is particularly important at $\frac{1}{2\pi}(\omega_m \pm \omega_{60}) \approx 260$ Hz, where the response is large, i.e., $g_{260} \approx 3(\frac{1}{2}aR)^{1/3}$ obtained from Eq. (2.7). Thus the measured phase response is given by

$$\phi = g_m \sin(\omega_m t - \chi_m) + g_{260}\sin(520\pi t - \chi_{260}). \tag{2.12}$$

Such effects are most important at f_m = 320 and 200 Hz. Figure 4 shows an example of the observed phase beating between the modulation frequency f_m = 320 Hz and the 260-Hz frequency at $\hat{B}_m$ = 4 G. The resulting response at 320 Hz agrees well with the formula in Eq. (2.9).

From these data, the amplitude of the 60-Hz ripple was found to be about $R \approx 5 \times 10^{-3}$. During the later runs for $\hat{B}_m$ = 2 G, the 60-Hz ripple was reduced by a 30 dB attenuator relative to the driving signal. The effect of

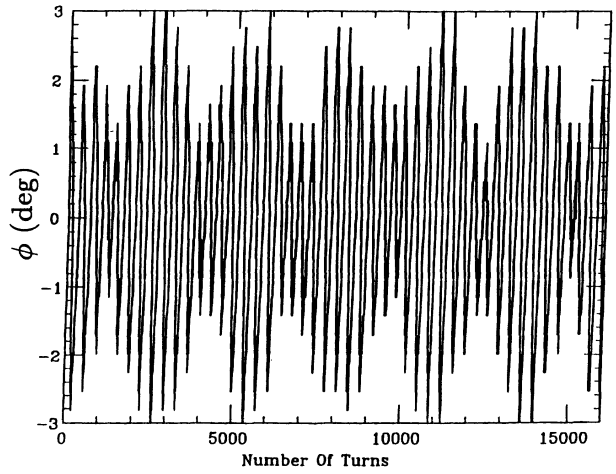

FIG. 4. The synchrotron phase measured from the phase detector at the modulation frequency of 320 Hz and modulation amplitude of $\hat{B}_m = 4$ G was plotted as a function of orbital revolutions at a ten-turn intervals. The beating of the synchrotron phase oscillations at 320 and 260 Hz arose from the 60-Hz ripple picked up from the cable run between the power supply and the modulation dipole.

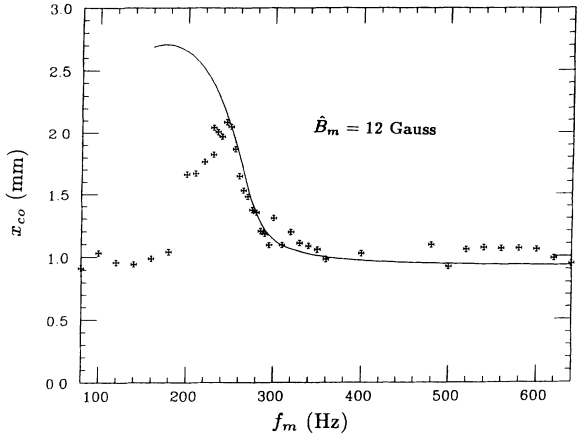

FIG. 5. The amplitude of the transverse closed-orbit oscillations as a function of the modulation frequency was fitted by using Eq. (2.16) including both the synchro-betatron coupling and the closed-orbit components. The modulation dipole field was 12 G.

the 60-Hz ripple was therefore reduced as shown in the lower parts of Fig. 3, where there was no peak in the phase response at modulation frequencies of 200 and 320 Hz.

D. The off-momentum closed-orbit analysis

The particle closed-orbit can be decomposed into a slow dipole induced closed-orbit modulation component and the off-momentum closed orbit resulting from the synchro-betatron coupling, i.e.,

$$x_{\rm co}(t) = x_d(t) + x_p(t) = X_m(s)\sin\omega_m t + D_x(s)\frac{\Delta p}{p}, \tag{2.13}$$

where

$$X_m(s) = \frac{\sqrt{\beta_x(s)\beta_x(s_0)}}{2\sin\pi\nu_x}\hat{\theta}\cos[\pi\nu_x - |\phi_x(s) - \phi_x(s_0)|], \tag{2.14}$$

and

$$\frac{\Delta p}{p} = \frac{\dot{\phi}}{h\eta\omega_0} - \frac{D_x(s_0)}{\eta C}\hat{\theta}\sin\omega_m t \approx \frac{\omega_m}{h\eta\omega_0}g\cos(\omega_m t - \chi) - \frac{\omega_s}{h\eta\omega_0}a\sin\omega_m t. \tag{2.15}$$

Since $\chi \approx \frac{\pi}{2}$ for the outer solution, the closed orbit is given by

$$x_{\rm co} \approx \left[X_m - \frac{D_x(s)}{h|\eta|\omega_0}(\omega_m g - \omega_s a)\right]\sin\omega_m t. \tag{2.16}$$

Using measured betatron amplitude function and dispersion function at a BPM location, Fig. 5 compares the calculated amplitude of the closed orbit with that of the measured data for $\hat{B}_m = 12$ G. Since the measured closed orbit corresponded to the centroid of the charge distribution of the bunch, the measured data deviated from Eq. (2.16) at frequencies below the bifurcation frequency. When the modulation frequency was far from the bifurcation frequency, the closed orbit arose mainly from the modulating dipole because the phase amplitude g resulting from the synchro-betatron coupling was small.

E. The effect of intrinsic rf phase noise

Since we were measuring the steady-state solution of the dissipative driven pendulum equation, any coherent synchrotron oscillation should have been completely damped. The damping time was about 0.33 s, therefore the coherent synchrotron motion should have been damped sufficiently at the end of 7 s. However, we observed consistently a 260-Hz coherent signal at all modulation frequencies. Figure 6 shows an example of a 520-Hz modulation at $\hat{B}_m = 12$ G. The upper part of Fig. 6 shows the Poincaré map of (ϕ, "$\frac{\Delta p}{p}$"), where "$\frac{\Delta p}{p}$" was obtained from the closed-orbit deviation, $x_{\rm co}$, divided by the dispersion function. The lower part shows the FFT of the phase oscillations.

The 260-Hz component had a phase amplitude about 56% of the 520-Hz modulation component shown in the lower part of Fig. 6. Such rf noise could be misidentified as period doubling. The measured phase amplitudes were respectively about 0.040 rad for the 520-Hz component and 0.023 rad for the 260-Hz component, which was consistently constant for all driving frequencies. Assuming that the 260-Hz component arose totally from rf phase noise, the magnitude of rf phase noise could be estimated by using solving Eq. (2.7), i.e., $a \approx (\frac{g}{3})^3 \approx 0.43$ μrad. The rf phase noise could arise from the rf system or from the high voltage power-supply ripple of the electron cooling system.

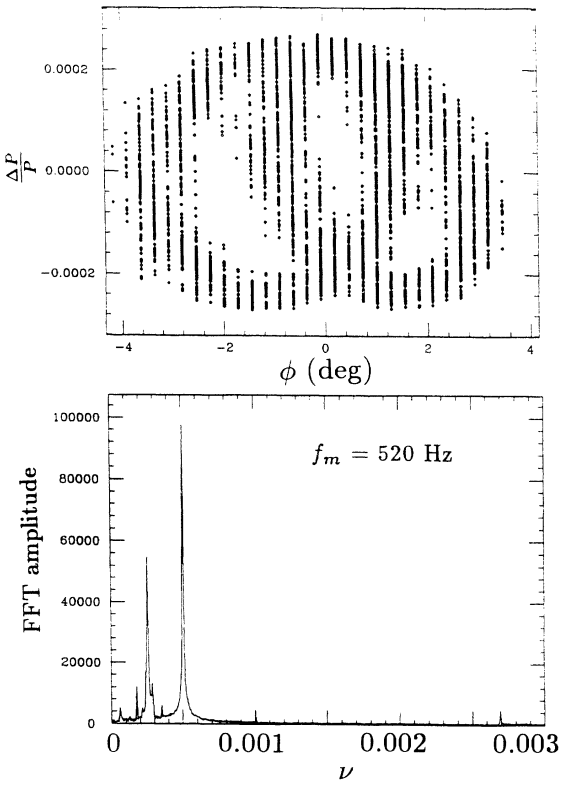

FIG. 6. The Poincaré map of the phase space, $(\phi, \text{“}\frac{\Delta p}{p}\text{”})$, measured at ten-turn intervals with $\hat{B}_m = 12$ G and $f_m = 520$ Hz is shown at the top. The FFT of the phase oscillation is shown at the bottom. The pattern resembles that of a period doubling. However, the essential mechanism here was not period doubling but rather arose from the rf noise at the synchrotron frequency. The 260-Hz noise was present at all modulation frequencies.

F. Numerical simulations

Numerical simulations have become a powerful tool in the study of nonlinear mapping equations. For a given initial phase-space coordinates, $(\phi_i, [\frac{\Delta p}{p}]_i)$, a particle obeying Eq. (2.3) will damp to an attractor solution due to the dissipative force. When the modulation frequency lies below the critical frequency ω_c, there exists two stable attractors. Figure 7 shows those initial phase-space coordinates converging toward the inner attractor (upper) and outer attractor (lower) for $f_m = 230$ Hz (left) and $f_m = 240$ Hz (right) with $B_m = 4$ G. The simulation results indicate that there are more initial phase-space points which converge toward the inner solution than the outer solution at 230 Hz, while the converse is true at 240 Hz. Such calculations confirm qualitatively the experimental data in Fig. 2.

It is interesting to note that those particles converging toward the inner (or the outer) attractor form nonintersecting intervolving spiral rings. To which attractor a particle will converge, depends sensitively on the initial phase-space coordinates, in particular for those particles located outside the bucket. It is worth pointing out that the orientation of initial phase-space coordinates which converge toward the inner or the outer attractor depends on the initial driving phase χ_0 of the dipole field in Eq. (2.1).

Numerical simulations indicate that all particles located initially inside the rf bucket will converge either to the inner or to the outer attractor. However, a small patch of initial phase-space coordinates located at the separatrix of the rf bucket converges toward two attractors moving along the separatrix. We do not yet understand the importance of this third attractor. Calculations of the Poincaré surface of section indicate that

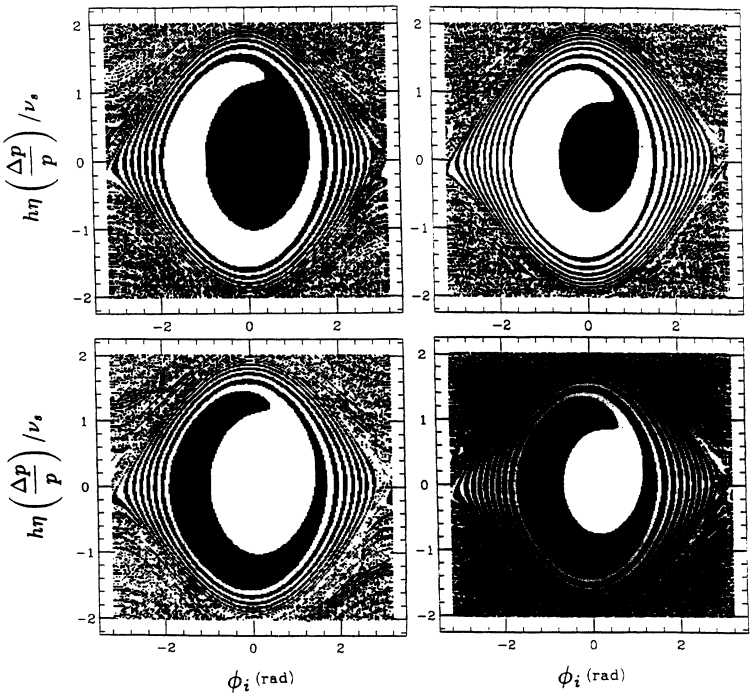

FIG. 7. The initial phase-space points, which damp to either the inner (upper graphs) or outer (lower graphs) attractors at modulation frequencies 230 Hz (left frames) and 240 Hz (right frames), obtained from numerical simulations are shown as black dots in phase space.

there are two stable fixed points and one unstable fixed point located at the separatrix of the rf bucket.

G. Melnikov function

The Melnikov function, which is a measure of the distance between two nearby trajectories, is usually used to test the chaotic bifurcation condition of a dynamical system [12]. In particular, when two trajectories, which pass through the hyperbolic fixed point, cross each other, the Melnikov function becomes zero in certain regions of the phase space. This gives rise to homoclinic structure and causes the onset of chaos in the dynamical system. The Melnikov function of Eq. (2.4) is given by

$$M(\theta_0) = \frac{\omega_s}{\omega_m}\left\{\pm\frac{2\pi\omega_m a}{\omega_s \cosh q\frac{\omega_m\pi}{2\omega_s}}\cos\frac{\omega_m\theta_0}{\omega_s} - \frac{16\alpha}{\omega_s}\right\} \quad (-\pi \le \theta_0 \le \pi), \tag{2.17}$$

which may become zero when the condition

$$a \ge \frac{8\alpha}{\omega_m\pi}\cosh\frac{\omega_m\pi}{2\omega_s} \tag{2.18}$$

is satisfied. Thus homoclinic structure can exist in this dynamical system with weak damping at a moderate modulation strength. The parameters used in this experiment did satisfy the condition of Eq. (2.18).

III. THE HAMILTONIAN FOR THE *rf* PHASE MODULATION THROUGH SB COUPLING

The Hamiltonian formalism is a powerful tool for understanding the dynamics of particle motion. With the normalized momentum variable defined as $\delta = \frac{h\eta}{\nu_s}(\frac{\Delta p}{p})$, the synchrotron equations of motion become

$$\phi_{n+1} = \phi_n + 2\pi\nu_s\delta_n + 2\pi\nu_s a\sin\nu_m\theta, \tag{3.1}$$

$$\delta_{n+1} = \delta_n - 2\pi\nu_s\sin\phi_{n+1} - 2\pi\frac{2\alpha}{\omega_0}\delta_n. \tag{3.2}$$

Neglecting the damping term by setting $\alpha = 0$, Eq. (3.2) can be derived from the following Hamiltonian

$$H = \frac{1}{2}\nu_s\delta^2 + \nu_s[1-\cos\phi] + \nu_s a\delta\sin\nu_m\theta, \tag{3.3}$$

where the orbital angle θ is used as the time variable. Transforming the phase-space coordinates (ϕ,δ) into the action-angle variables (J,ψ) discussed in the Appendix, the Hamiltonian becomes

$$H = H_0(J) + H_1(J,\psi,\theta), \tag{3.4}$$

where the unperturbed Hamiltonian is $H_0(J) = \nu_s J - \frac{\nu_s}{16}J^2 + \cdots$, and the perturbation is given by

$$H_1 = -\frac{\sqrt{2J}}{2}\nu_s a[\sin(\psi-\nu_m\theta) - \sin(\psi+\nu_m\theta)] + \cdots. \tag{3.5}$$

The external dipole modulation induces a synchrotron phase modulation, which gives rise to resonances when the modulation frequency equals an odd multiple of the synchrotron frequency, i.e., $\nu_m \approx (2k+1)\nu_s$. These resonances, created by the external modulations at harmonics of frequencies intrinsic to the system, are usually called the parametric resonances.

A. Tori near the first-order synchrotron resonance

When the modulation frequency is close to an odd multiple of the synchrotron frequency, the parametric resonance term in Eq. (3.5) becomes important. As an example, we consider the resonance near the first harmonic, i.e., $\nu_m \approx \nu_s$. To gain insight into the Hamiltonian flow, we transform the coordinate system to the resonance precessing frame using the generating function,

$$F_2(\psi,\tilde{J}) = \left(\psi - \nu_m\theta - \frac{\pi}{2}\right)\tilde{J}. \tag{3.6}$$

The coordinates are transformed according to $\tilde{\psi} = \psi - \nu_m\theta - \frac{\pi}{2}$, $J = \tilde{J}$. The new Hamiltonian becomes

$$\tilde{H} \approx (\nu_s-\nu_m)\tilde{J} - \frac{\nu_s}{16}\tilde{J}^2 - \frac{\nu_s a\sqrt{2\tilde{J}}}{2}\cos\tilde{\psi} + \Delta H(\tilde{J},\tilde{\psi},\theta). \tag{3.7}$$

The time-dependent part of the perturbation, ΔH, oscillates at the frequency of $2\nu_m$ with

$$\Delta H \approx \frac{\nu_s a\sqrt{\tilde{J}}}{\sqrt{2}}\cos(\tilde{\psi} + 2\nu_m\theta) + \cdots. \tag{3.8}$$

Because of the stationary phase (or resonance) condition, $\frac{d\tilde{\psi}}{d\theta} \approx 0$, the time-independent part of the Hamiltonian contributes coherently to the perturbing kicks. Thus the particle motion is strongly perturbed by the external modulation force through the resonance condition. The particle trajectory in phase space can be described by the torus of the time-averaged Hamiltonian [8],

$$\langle H\rangle = (\nu_s-\nu_m)\tilde{J} - \frac{\nu_s}{16}\tilde{J}^2 - \frac{\nu_s a\sqrt{2\tilde{J}}}{2}\cos\tilde{\psi}, \tag{3.9}$$

which is an invariant. Particle trajectories follow the tori of the Hamiltonian flow. Tori with constant Hamiltonian values are shown in Fig. 8 for $\frac{\nu_m}{\nu_s} = 0.935$ and $a = 0.02$. Hereafter, we drop the tilde notation for simplicity. The equation of motion for the Hamiltonian flow becomes

$$\dot{J} = -\frac{1}{2}\nu_s a\sqrt{2J}\sin\psi, \tag{3.10}$$

$$\dot{\psi} = (\nu_s-\nu_m) - \frac{\nu_s}{8}J - \frac{\nu_s a}{2\sqrt{2J}}\cos\psi. \tag{3.11}$$

The fixed points of the Hamiltonian are given by $\dot{J} = 0$, $\dot{\psi} = 0$. Let the phase coordinate of the fixed point be $g = \sqrt{2J}\cos\psi$ with $\psi = 0$ or π. We find that g satisfies the following equation:

$$\frac{1}{16}g^3 - (1-\frac{\nu_m}{\nu_s})g + \frac{a}{2} = 0, \tag{3.12}$$

which is identical to Eq. (2.7) at $\nu_m \approx \nu_s$ and $\alpha = 0$.

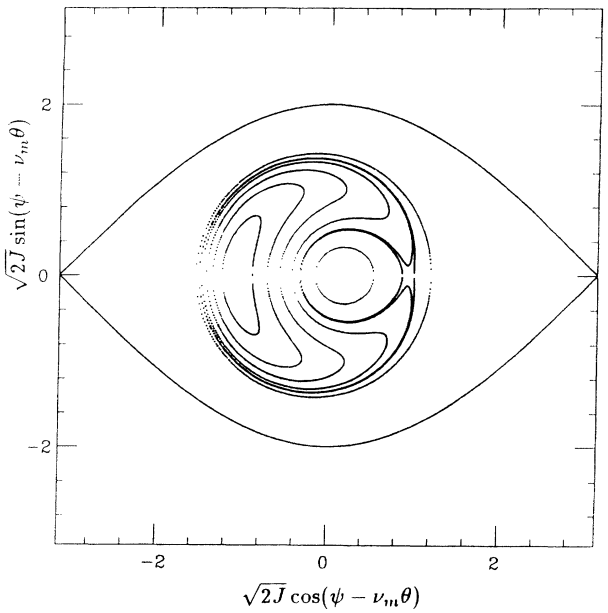

FIG. 8. The Poincaré surface of section is shown for $f_m = 245$ Hz and $f_s = 262$ Hz at $a = 0.02$.

Therefore the attractor solutions, discussed in Sec. II, are fixed points of the time averaged Hamiltonian. A weak damping force does not destroy the resonance island created by the external rf phase modulation. Because of the phase-space damping, these fixed points of the Hamiltonian become attractors. Particles in the phase space are damped incoherently toward these attractors. The steady-state solutions shown in Figs. 1 and 3 correspond to two stable fixed points (SFP's) and one unstable fixed point (UFP). As the damping force becomes larger, the outer SFP and the UFP may collide and disappear. Figure 1 shows that the outer SFP disappears at frequency below 253 Hz for $\alpha \geq 10\ \mathrm{s}^{-1}$.

When the modulation frequency ν_m is less than ν_c, where ν_c is called the bifurcation tune given by

$$\nu_c = \nu_s\left[1 - \frac{3}{16}(4a)^{2/3}\right], \tag{3.13}$$

there are three solutions to Eq. (3.12) given by

$$\begin{aligned} g_a(x) &= -\frac{8}{\sqrt{3}}x^{1/2}\cos\frac{\xi}{3}, \\ g_b(x) &= \frac{8}{\sqrt{3}}x^{1/2}\sin\left(\frac{\pi}{6} - \frac{\xi}{3}\right), \\ g_c(x) &= \frac{8}{\sqrt{3}}x^{1/2}\sin\left(\frac{\pi}{6} + \frac{\xi}{3}\right), \end{aligned} \tag{3.14}$$

where

$$\begin{aligned} x &= 1 - \frac{\nu_m}{\nu_s}, \\ x_c &= 1 - \frac{\nu_c}{\nu_s}, \\ \xi &= \arctan\sqrt{\left(\frac{x}{x_c}\right)^3 - 1}, \end{aligned}$$

with $\nu_m \leq \nu_c$ or $\frac{x}{x_c} \geq 1$. The solutions g_a with $\psi = \pi$ and g_b with $\psi = 0$ are SFP's and the solution g_c with $\psi = 0$ is the UFP. Stable tori in phase space are closed curves around the SFP's. The particle motion in phase space can be described by the tori of constant Hamiltonian around SFP's shown as an example in Fig. 8 for $f_m = 245$ Hz and $f_s = 262$ Hz with $a = 0.02$.

Figure 9 shows fixed-point solutions [Eq. (3.14)] normalized by $\frac{g}{(4a)^{1/3}}$, as a function of $(\frac{x}{x_c})^{1/2}$ for $x \geq x_c$. Other solid lines will be discussed later. The longitudinal beam profiles obtained from the sum signal of a BPM shown in Fig. 2 at modulation frequencies below 250 Hz are particles trapped in islands around SFP's, which rotate coherently at the modulation frequency. The distribution function of these beamlets will conform to the local potential well. Because the local potential well is not uniform (see Fig. 8), these beamlets, shaped like an elongated ellipse, will display a high peak current at both extremes of the phase coordinate.

In the limiting condition $\nu_m \ll \nu_c$, we have $\xi \to \frac{\pi}{2}$, $g_a \to -4x^{1/2}$, $g_c \to 4x^{1/2}$, $g_b \to 0$, where the phase-space area of the island around the outer SFP is small in comparison with that of the island around the inner SFP. When the modulation frequency is increased, the phase-space area of the outer island increases while that of the inner island decreases. As the modulation frequency approaches the bifurcation frequency from below, the UFP and the outer SFP move in and the inner SFP moves out. At the bifurcation frequency, where $\xi = 0$, the UFP coincides with the inner SFP with the phase amplitude $g_b = g_c = (4a)^{1/3}$ and the phase-space area of the inner island becomes zero.

Beyond the bifurcation frequency, $\nu_m > \nu_c$, there is only one real solution to Eq. (3.12) given by

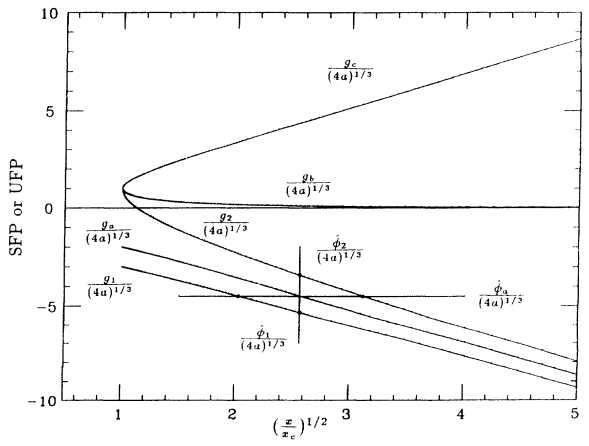

FIG. 9. The stable and unstable fixed points of the Hamiltonian are shown as a function of the modulation frequency in terms of $(\frac{x}{x_c})^{1/2}$ defined in Eq. (3.14). The intercepts of the separatrix with the phase coordinate are also shown. For a given phase amplitude of the beam bunch $\hat{\phi}$, bunch dilution may occur for phase modulation frequencies between (ν_2, ν_1).

$$g_a = -(4a)^{1/3}\left\{\left[\sqrt{1-\left(\frac{x}{x_c}\right)^3}+1\right]^{1/3} - \left[\sqrt{1-\left(\frac{x}{x_c}\right)^3}-1\right]^{1/3}\right\}, \quad (3.15)$$

and all tori are closed curves orbiting about the outer SFP. The longitudinal beam profile shown in Fig. 2 at $f_m = 260$ Hz corresponds to a single beamlet orbiting about the outer SFP, where the accumulated beam profile measured with an oscilloscope exhibited also a smaller peak current when the beamlet rotated to the center of the bucket, or the center of the phase coordinate.

B. Hysteresis of resonant islands

The hysteresis phenomena discussed in Sec. II B can be explained based on the resonant islands of SFP's. At a modulation frequency above the bifurcation frequency, there is only one SFP given by Eq. (3.15). When the modulation frequency is ramped adiabatically downward through the bifurcation frequency, the amplitude of the synchrotron oscillations follows the outer SFP toward a large amplitude. When the phase-space area of the outer island becomes too small to contain the bunch (see Fig. 8), the synchrotron oscillations will jump from the outer SFP to the inner SFP.

At a modulation frequency far below the bifurcation frequency, the size of the outer island is either nonexistent or very small and the beam populates mainly the inner island. When the modulation frequency is ramped up toward the bifurcation frequency, the beam bunch will follow adiabatically the inner SFP until the size of the inner island becomes too small to hold the beam bunch. Thus the hysteretic phenomena observed are related to the bifurcation of fixed points due to the nonlinearity of the parametric resonance system.

C. The equilibrium distribution of beamlets and the island tune

In the presence of dissipative and diffusive processes, the equilibrium beam size is determined by the balance of the dissipative and the diffusive forces. At the IUCF Cooler Ring, the damping force came from the drag force of the Coulombic interaction between protons and the cold electron beam in the electron cooling region while the diffusive processes could result from the instabilities due to impedances, intrabeam Coulomb scattering, beam gas scattering, and noise in accelerator devices, etc. However, the beam profile, which satisfies the Vlasov equation is determined by the external potential well at a fixed point of the Hamiltonian and possibly also by the mean field of the beamlet, e.g., the potential well distortion. Small-amplitude oscillations about a fixed point can be obtained by making a local coordinate expansion of the action-angle variables. Let y, p_y be local coordinates about a fixed point of the Hamiltonian, i.e.,

$$y = \sqrt{2J}\cos\psi - g, \quad p_y = -\sqrt{2J}\sin\psi, \quad (3.16)$$

where g is a fixed point. The Hamiltonian becomes

$$H = \frac{\nu_s a}{4g}\left(1-\frac{g^3}{4a}\right)y^2 + \frac{\nu_s a}{4g}p_y^2 + \cdots. \quad (3.17)$$

This implies that the fixed point g is a SFP if $1-\frac{g^3}{4a} \geq 0$ or conversely the fixed point g is a UFP if $1-\frac{g^3}{4a} < 0$. Because $\frac{g_a^3}{4a} < 0$ and $\frac{g_b^3}{4a} \leq 1$, both g_a and g_b are SFP's. On the other hand, $\frac{g_c^3}{4a} \geq 1$, so g_c is the UFP. The island tune for a small amplitude oscillation in Eq. (3.17) around a fixed point is given by

$$\nu_{\text{island}} = \left|\nu_s - \frac{\nu_s g^2}{16} - \nu_m\right|\left(1-\frac{g^3}{4a}\right)^{1/2}. \quad (3.18)$$

In the limit that $\frac{g^3}{4a} \ll 1$, Eq. (3.18) also implies that the solution of the Hamiltonian can be expressed in terms of a linear superposition of the homogeneous and inhomogeneous solutions [8].

The equilibrium beam profile, which satisfies the Vlasov equation, is a function of the Hamiltonian of Eq. (3.17). Assuming a Gaussian distribution, we obtain

$$\rho(y,p_y) = \frac{\sqrt{1-\frac{g^3}{4a}}}{2\pi\sigma_0^2} e^{-(1-\frac{g^3}{4a})\frac{1}{2\sigma_0^2}y^2 - \frac{1}{2\sigma_0^2}p_y^2}. \quad (3.19)$$

Since each particle in the steady state rotates in the phase space at the modulation frequency, the beam profile will retain its shape except for the exchange of the local coordinates. The observed longitudinal profile, which corresponds to the line density of the bunch, is obtained by integrating the local momentum coordinate, i.e.,

$$\rho(y) = \int \rho(y,p_y)dp_y, \quad (3.20)$$

which leads to the line density of Eq. (2.10) with the effective bunch width modulating at the modulation frequency. The aspect ratio (the ratio between the width and height) of the ellipse is given by $\sqrt{1-\frac{g^3}{4a}}$, which agrees well with data.

D. The separatrix and the bunch dilution due to the rf phase modulation

The torus which passes through the UFP is called the separatrix. Stable tori about resonance islands are separated by the separatrix, which is given by phase-space coordinates (J,ψ), satisfying

$$\frac{H(J,\psi)}{\nu_s} = \frac{x}{2}g_c^2 - \frac{1}{64}g_c^4 - \frac{a}{2}g_c, \quad (3.21)$$

with $x = 1-\frac{\nu_m}{\nu_s}$ and the UFP g_c given by Eq. (3.14). The separatrix intercepts the phase coordinate at g_1 and g_2, which can be obtained by solving Eq. (3.21). Using the notation $h_i = \frac{g_i}{(4a)^{1/3}}$, i.e., $h_1 = \frac{g_1}{(4a)^{1/3}}$, $h_2 = \frac{g_2}{(4a)^{1/3}}$, $h_c = \frac{g_c}{(4a)^{1/3}}$ etc., the solutions of Eq. (3.21) are given by

$$h_1 = -h_c - \frac{2}{\sqrt{h_c}}, \quad h_2 = -h_c + \frac{2}{\sqrt{h_c}}. \tag{3.22}$$

Figure 9 shows the phase amplitudes, h_a, h_b, h_c, h_1, and h_2, of fixed points and the intercepts of the separatrix as a function of $(\frac{x}{x_c})^{1/2}$ at $\frac{x}{x_c} \geq 1$. The location that the separatrix cuts through the origin of the phase space is $\frac{x}{x_c} = 2^{1/3}$ with $h_c = 2^{2/3}$. In the intermediate region, $1 \leq (\frac{x}{x_c})^{1/2} \leq 5$, h_a, h_b, and h_c can be approximated well with

$$\begin{aligned} h_a &\approx -1.650(\tfrac{x}{x_c})^{1/2} - 0.350, \\ h_1 &\approx -1.575(\tfrac{x}{x_c})^{1/2} - 1.425, \\ h_2 &\approx -1.889(\tfrac{x}{x_c})^{1/2} + 1.445. \end{aligned} \tag{3.23}$$

Asymptotically at $(\frac{x}{x_c})^{1/2} \gg 1$, we have

$$|h_a| \approx |h_c| \approx |h_1| \approx |h_2| \sim \sqrt{3}\left(\frac{x}{x_c}\right)^{1/2}.$$

For a beam bunch with a phase amplitude $\hat{\phi}$ (the corresponding phase-space area is $\pi\hat{\phi}^2$ in normalized coordinates), the normalized phase amplitude of the bunch is $\hat{h} = \frac{\hat{\phi}}{(4a)^{1/3}}$ shown schematically as the horizontal line in Fig. 9, which intersects the h_1, h_a, and h_2 curves at the modulation frequencies given approximately by

$$\begin{aligned} \frac{\nu_a}{\nu_s} &= 1 - 0.0689(4a)^{2/3}(\hat{h} - 0.350)^2, \\ \frac{\nu_1}{\nu_s} &= 1 - 0.0756(4a)^{2/3}(\hat{h} - 1.425)^2, \\ \frac{\nu_2}{\nu_s} &= 1 - 0.0525(4a)^{2/3}(\hat{h} + 1.445)^2. \end{aligned} \tag{3.24}$$

When the modulation frequency is smaller than ν_2, the separatrix is outside the bunch area, and the phase modulation will have little effect on the beam. When the modulation frequency is larger than ν_1, the separatrix is completely inside the bunch area, therefore the bunch area will not be affected. When the modulation frequency lies between $\nu_2 \leq \nu_m \leq \nu_1$, particles having the phase amplitude greater than $\hat{\phi}_2$, given by $\frac{\hat{\phi}_2}{(4a)^{1/3}} = h_c - \frac{2}{\sqrt{h_c}}$, will oscillate about the fixed point g_a of the island and reach the maximum oscillation amplitude of $\frac{\hat{\phi}_1}{(4a)^{1/3}} = h_c + \frac{2}{\sqrt{h_c}} \approx |h_a| + \frac{2}{\sqrt{|h_a|}}$. Therefore the percentage growth of the bunch area is

$$G = \frac{8}{h_c^{3/2}} = 8\left(\frac{4a}{\hat{\phi}^3}\right)^{1/2}. \tag{3.25}$$

Demanding the phase-space area growth to be less than 50%, we obtain the tolerance criterion of the rf phase modulation as follows:

$$a \leq \frac{\hat{\phi}^3}{4^5} \approx \frac{\sigma_\phi^3}{70} \tag{3.26}$$

for the modulation frequency at $\nu_m = \nu_2$. Modulation frequencies lying below ν_2 do not produce strong perturbation to the beam. Note here that those particles within the core of the bunch, i.e., $\phi \leq \hat{\phi}_2$, are not affected by the rf phase modulation. It is worth emphasizing that the validity of Eqs. (3.23) and (3.24) are limited by the condition $\frac{x}{x_c} \leq 25$. Application of these equations should be checked carefully.

E. The tolerance of the SSC beams to ground vibrations

During the acceleration of the SSC beam from 2 TeV to 20 TeV, the synchrotron frequency sweeps from 7 to 4 Hz. Unless there is a strong resonant ground vibration wave in this frequency range, we expect that the constraint is most severe at the storage mode. In the storage mode at 20 TeV, the rf parameters are the rf voltage $V_0 = 20$ MV, the harmonic number $h = 104\,544$, the circumference $C = 87\,120$ m, the momentum compaction factor 9.1×10^{-5}, and the synchrotron frequency $f_s = 4.13$ Hz. The bucket area is 18.34 eV s and the 95% bunch area is 4.4 eV s. The bunch length is $\sigma_s = 6.0$ cm or $\sigma_\phi = 4.1°$ and the momentum spread is $\sigma_\delta = 0.58 \times 10^{-4}$. The 95% phase amplitude of the beam is given by $\hat{\phi} = \sqrt{6}\sigma_\phi = 10°$. Using the criterion of Eq. (3.26), the tolerable modulation amplitude is given by $a \leq 5 \times 10^{-6}$.

Let us consider the contribution of a single arc quadrupole to the synchro-betatron coupling caused by a displacement of Δx. The phase shift parameter a is given by

$$a \approx \frac{\omega_0}{2\pi\omega_s} 2\pi h \frac{\Delta x}{f_q} \frac{\langle D_x \rangle}{C} \approx 2.4 \times 10^{-5} \Delta x \ [\mu\text{m}], \tag{3.27}$$

where the focal length of a quadrupole is $f_q \approx 62.5$ m and the average dispersion function is $\langle D_x \rangle \approx 1.3$ m.

The dominant ground vibration amplitude from a quarry blast has been measured [4] to be about 0.143 μm at 1 Hz and 0.108 μm at 3 Hz. The phase modulation amplitude arising from the 3-Hz component is about $a_{QB} \approx 7.2 \times 10^{-5}$ by taking the statistical sum of 1000 quadrupoles. At such a small amplitude, the 3-Hz phase modulation may not couple strongly to the SSC beam because the separatrix of the modulating islands is outside the phase-space area of the bunch. The dangerous modulating frequency lies within 4.11 to 4.12 Hz [see Eq. (3.24)] for the synchrotron frequency of 4.13 Hz. In order to maintain a less than 50% phase area growth, the tolerable ground vibration amplitude is $\Delta x \leq 0.007$ μm integrating over a range of $\Delta f = 0.01$ Hz from the modulation frequency of 4.11 to 4.12 Hz.

Similarly, the frequency spectrum arising from a train crossing is a broad spectrum around 3 Hz and 7 Hz. The 3 Hz does not affect the beam while the phase modulation at 7 Hz may affect the SSC beam during the injection. If we assume that 10 quadrupoles will contribute coherently to the phase modulation during a train crossing [13], the phase modulation amplitude becomes $a_{TC} = 1.2 \times 10^{-5}$ with $\Delta x = 0.058$ μm. The effective phase-space area growth given by Eq. (3.25) will be about G =75%. Active compensation by using rf systems might ease or solve some problems of phase-space dilution.

F. The effect of power-supply ripple on the RHIC beams

For RHIC, the circumference is 3833.84 m with transition energy $\gamma_T = 23.6$. The parameters for the accelerating rf cavity are $h = 342, V = 300$ kV, and the synchronous phase $\phi_0 = 0.161$ rad. The acceleration rate is $\dot{\gamma} = 1.6\ \mathrm{s}^{-1}$. The beam crosses 60 Hz at about $\gamma = 17.5$. The 95% phase-space area is 0.3 eV s with rms momentum spread 0.0005 and rms phase spread $\sigma_\phi = 0.33$ rad. The rate change of the synchrotron tune is $\frac{d\nu_s}{dt} \approx -1.9 \times 10^{-4}\ \mathrm{s}^{-1}$ or -2.4×10^{-9} per revolution. Figure 10 shows the separatrixes at $a = 0.001$ for $\frac{f_m}{f_s} = 0.95$ (curve 1) and 0.995 (curve 2).

When the beam energy is accelerated toward the transition energy, the synchrotron frequency decreases toward the 60-Hz ripple modulation frequency and thus the fixed points of the synchrotron Hamiltonian with the 60-Hz phase modulation move inward as shown in Fig. 11. At the synchrotron frequency f_2 where the inner intercept g_2 of the separatrix equals the phase amplitude of the bunch ($\sqrt{6}\sigma_\phi = 0.80$ rad), the beam particles begin to be affected. Once the synchrotron frequency becomes lower than f_1, where the outer intercept g_1 of the separatrix lies inside the bunch width, the phase modulation will not affect the bunch area of the beam. Figure 12 shows f_1 and f_2 as a function of the modulation amplitude a for $\hat{\phi} = 0.80$ rad. Note here that Eqs. (3.23) and (3.24) are not applicable for $a \leq 0.000\,25$. At a small modulation amplitude $a \to 0$, we find that f_1 and f_2 become a single frequency given by

$$f_1 = f_2 = 60 \Big/ \left(1 - \frac{\hat{\phi}^2}{16}\right).$$

The time required for the bunch to be accelerated through synchrotron frequencies f_1 and f_2 is about 100–300 ms depending on the phase modulation amplitude a. When the acceleration rate is fast, particles do not have enough time to follow the separatrix and therefore the increase in the bunch area is small. When the acceleration rate is small, particles can move along the separatrix and reach large amplitudes. The increase in the phase amplitude is given approximately by $2.8(4a)^{1/3}$ obtained from Eq. (3.23). Allowing the phase-space area to increase by a factor of 2, we obtain the condition $2.8(4a)^{1/3} \leq \frac{1}{2}\sqrt{6}\sigma_\phi$ or

$$a \leq \frac{\sigma_\phi^3}{48} \approx 7.5 \times 10^{-4}.$$

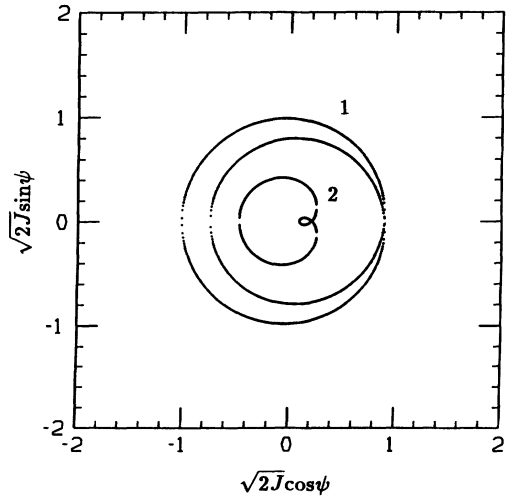

FIG. 10. The separatrixes for the Hamiltonian of Eq. (3.9) with $a = 0.001$ and $\frac{f_m}{f_s} = 0.95$ (curve 1) and 0.995 (curve 2).

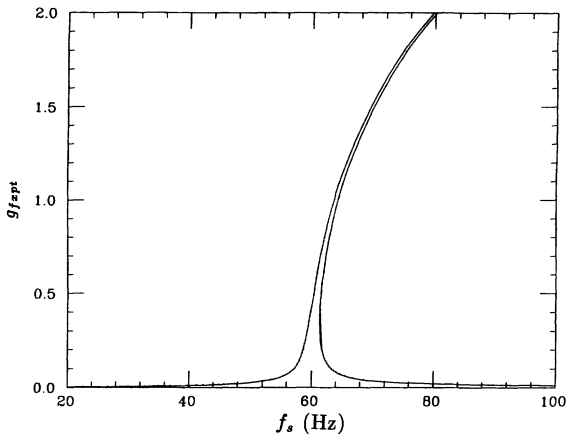

FIG. 11. The fixed points for $f_m = 60$ Hz as a function of the synchrotron frequency f_s for $a = 0.01$.

The synchrotron frequency ramps through 60 Hz at 17 GeV/c for heavy-ion beams. Assuming that power-supply ripple contributes an error ε to all dipoles, the resulting path length difference will be $\Delta C = \langle D_x \rangle 2\pi\varepsilon$, where the average dispersion function at the dipole location is $\langle D_x \rangle \approx 1$ m. Thus the amplitude of the rf phase shift per turn is $\Delta\hat{\phi} \approx 3.52\varepsilon$. The resulting phase shift parameter becomes,

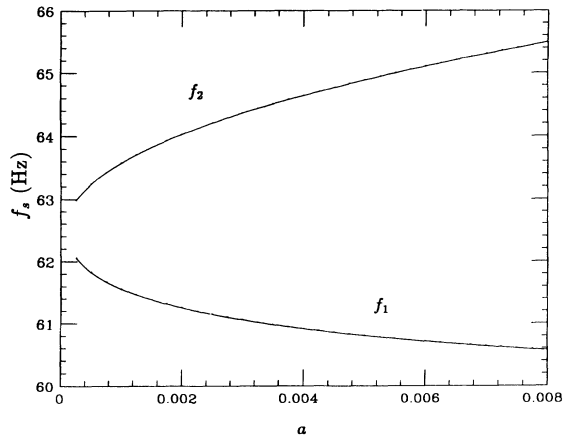

FIG. 12. The synchrotron frequency f_2 where the separatrix touches the bunch area occupied by the RHIC beam and the frequency f_1 at which the separatrix is completely inside the RHIC beam are shown as a function modulation amplitude a at 60-Hz modulation frequency. The phase amplitude of the bunch used is $\hat{\phi} = 0.80$ rad.

$$a = \frac{\omega_0}{2\pi\omega_s}\hat{\Delta\phi} \approx 730\ \varepsilon.$$

If the power-supply ripples of all dipoles are in phase, the phase modulation amplitude may be large. At the level of $\varepsilon = 10^{-6}$, the resulting phase modulation amplitude is $a = 7.3 \times 10^{-4}$ rad, which is at the tolerable limit discussed earlier. At $\varepsilon = 10^{-5}$, the phase modulation problem can be alleviated by designing the power-supply bus to cancel the effect of ripple via reversing the phase of power-supply ripple in each arc. With proper cancellation, the resulting synchro-betatron coupling can be suppressed.

It is fortunate that the synchrotron frequency stays below the 60-Hz modulation frequency after the transition energy crossing. If the synchrotron frequency were ramped through the modulation frequency from below, the resonance island created by the phase modulation would transport particles from a small synchrotron amplitude outward. The growth of phase-space area would be much worse in this later case [11]. On the other hand, ramping the rf phase modulation frequency through the synchrotron frequency from above may be used effectively for the bunched beam dilution.

IV. CONCLUSION

We found that the synchro-betatron coupling resonance in a proton storage ring can be induced by dipole modulation at frequencies near the synchrotron frequency. Due to the weak dissipative force of the electron cooling at the IUCF Cooler Ring, the beam particles were found to converge toward attractors of the dissipative parametric resonant system. These attractors were found to orbit about the center of the bucket at the modulation frequency displaying the coherent nature of the dynamical system. The transverse dipole-field modulation resulted in a very unusual bunch shape distribution in the longitudinal phase space. Data observed with an oscilloscope revealed that the bunch split into two beamlets located at amplitudes corresponding to the stable fixed points of the Hamiltonian. The experimental data agreed well with the synchro-betatron coupling analysis.

Numerical simulations were performed to test the damping mechanism of the dissipative resonant equation. We found that the initial phase-space coordinates which converge to the inner or the outer attractor form nonintersecting spiral rings.

Based on our experimental data, synchro-betatron coupling effects due to ground vibration for the SSC and the power-supply ripple for RHIC have been studied. We found that the effects of the synchro-betatron coupling due to power-supply ripple with amplitude 10^{-6} for RHIC resulted in a tolerable longitudinal phase-space dilution of about a factor of 2. At the power-supply ripple amplitude of 10^{-5}, the effects should be corrected by reversing the power-supply ripple phase in different arcs. The effect of ground vibration on the beam dynamics for the SSC beam has also been analyzed. We found that if the modulation frequency is 4.12 Hz then the tolerable quadrupole vibration (50% emittance dilution) is about 0.007 μm, which includes statistical enhancement of 1000 quadrupoles. At a lower modulation frequency, the beam will not be strongly affected. The effect of train crossing is more important to the SSC beam at the injection energies. In reality, some ground vibration effects are adiabatic. Particle motion may follow the Hamiltonian flow adiabatically without diluting the bunch phase-space area. The effects of phase-space dilution due to the synchro-betatron coupling could be overcome by an active feedback rf system. Experiments testing these ideas are being planned. In this paper we did not discuss the beam diffusion due to nonresonant rf phase noise induced by ground vibration or the power-supply ripple. Such a process can be estimated by the well-established rf diffusion theory [14].

ACKNOWLEDGMENT

This work was supported in part by a grant from NSF No. PHY-9221402 and from the U.S. DOE No. DE-FG02-93ER40801.

APPENDIX A: THE ACTION ANGLE OF THE UNPERTURBED HAMILTONIAN

Let the unperturbed Hamiltonian and its perturbation of Eq. (3.3) be given by

$$H_0 = \frac{1}{2}\nu_s\delta^2 + 2\nu_s \sin^2\frac{\phi}{2}, \tag{A1}$$

$$H_1 = \nu_s a\delta \sin\nu_m\theta. \tag{A2}$$

Here ν_s is the synchrotron frequency at zero synchrotron amplitude. The action-angle variables of the unperturbed Hamiltonian can be expressed in terms of the complete elliptical integral of the first kind to be discussed in the following [10]. Expressing the synchrotron coordinates in parameters k, w as

$$\sin\frac{\phi}{2} = k\sin w, \quad \frac{\delta}{2} = k\cos w, \tag{A3}$$

one obtains $H_0 = 2\nu_s k^2$ with $0 \le k \le 1$. The relation between the parameter w and the synchrotron phase angle will become clear later. Using the definition of Eq. (A3), the action of the unperturbed Hamiltonian is given by

$$J = \frac{1}{2\pi}\oint \delta d\phi = \frac{8}{\pi}[E(k) - (1-k^2)K(k)], \tag{A4}$$

where the complete elliptical function is given by

$$E(k) = \int_0^{\frac{\pi}{2}} \sqrt{1 - k^2\sin^2 w}\, dw,$$

$$K(k) = \int_0^{\frac{\pi}{2}} \frac{1}{\sqrt{1 - k^2\sin^2 w}} dw.$$

The angle variable conjugate to the action J can be obtained from Hamilton's equation of motion, i.e.,

$$\dot{\psi} = \frac{\partial H_0}{\partial J} = \nu_s \frac{\pi}{2K(k)}, \tag{A5}$$

where we have used the identities

$$2k^2\frac{dE(k)}{dk^2} = E(k) - K(k),$$
$$2k^2\frac{dK(k)}{dk^2} = \frac{1}{1-k^2}E(k) - K(k).$$

Now the task is to expand the momentum coordinate δ in Fourier harmonics of the conjugate angle variable ψ given by

$$\psi = \frac{\pi\nu_s}{2K(k)}\theta + \psi_0. \tag{A6}$$

Using $\dot{\phi} = \nu_s\delta$, the relation between the orbital angle θ and the parameter w is given by

$$\nu_s(\theta - \theta_0) = \int_{\phi_0}^{\phi}\frac{d\phi}{\delta} = u - u_0, \tag{A7}$$

where

$$u = \int_0^w \frac{1}{\sqrt{1-k^2\sin^2 w'}}dw',$$
$$u_0 = \int_0^{w_0} \frac{1}{\sqrt{1-k^2\sin^2 w'}}dw'. \tag{A8}$$

Here the Jacobian elliptical function is then defined as

$$\sin w = \mathrm{sn}(u|k), \quad \cos w = \mathrm{cn}(u|k). \tag{A9}$$

Thus the expansion of $\delta = 2k\ \mathrm{cn}(u|k)$ in Fourier harmonics of ψ can be obtained from the formula of Eq. (16.23.2) in reference [10], i.e.,

$$\mathrm{cn}(u|k) = \frac{2\pi}{kK(k)}\sum_0^\infty \frac{q^{n+1/2}}{1+q^{2n+1}}\cos(2n+1)\psi, \tag{A10}$$

where the parameter q is given by [see Eq. (17.3.21) of Ref. [10]],

$$q = e^{-\pi K'/K} = \frac{k^2}{16} + 8\left(\frac{k^2}{16}\right)^2 + 84\left(\frac{k^2}{16}\right)^3 + 992\left(\frac{k^2}{16}\right)^4 + \cdots.$$

Using power-series expansion of the elliptical integrals, i.e.,

$$K(k) = \frac{\pi}{2}\left[1 + \left(\frac{1}{2}\right)^2 k^2 + \left(\frac{1\times 3}{2\times 4}\right)^2 k^4 + \left(\frac{1\times 3\times 5}{2\times 4\times 6}\right)^2 k^6 + \cdots\right],$$
$$E(k) = \frac{\pi}{2}\left[1 - \left(\frac{1}{2}\right)^2 \frac{k^2}{1} - \left(\frac{1\times 3}{2\times 4}\right)^2 \frac{k^4}{3} - \left(\frac{1\times 3\times 5}{2\times 4\times 6}\right)^2 \frac{k^6}{5} - \cdots\right],$$

one obtains

$$J = 2k^2\left(1 + \frac{1}{8}k^2 + \frac{3}{64}k^4 + \cdots\right), \tag{A11}$$
$$k^2 = \frac{J}{2}\left(1 - \frac{1}{16}J - \frac{1}{256}J^2 - \cdots\right), \tag{A12}$$
$$2k\mathrm{cn}(u|k) = (2J)^{1/2}\cos\psi + \frac{(2J)^{3/2}}{64}\cos 3\psi + \frac{(2J)^{5/2}}{4096}\cos 5\psi + \cdots. \tag{A13}$$

Substituting the elliptical cosine function into the perturbation, one obtains

$$H_1(J,\psi) \approx \nu_s a\left[(2J)^{1/2}\cos\psi + \frac{(2J)^{3/2}}{64}\cos 3\psi + \cdots\right]\sin\nu_m\theta. \tag{A14}$$

[1] E.M. McMillan, Phys. Rev. **68**, 143 (1945); V.I. Veksler, C. R. Acad. Sci. U.S.S.R. **43**, 329 (1944); **44**, 365 (1944).

[2] E.D. Courant and H.S. Snyder, Ann. Phys. (N.Y.) **3**, 1 (1958).

[3] M.C. Crowley-Milling and I.I. Rabinowitz, IEEE Trans. Nucl. Sci. **NS18**, 1052 (1971); SPEAR group, *ibid.* **NS22**, 1366 (1975); A. Piwinski, *ibid.* **NS24**, 1408 (1977); A Piwinski, in *Proceedings of 11th International Conference on High Energy Accelerators* (CERN, Geneva, 1980), p. 754; A. Piwinski, in CERN Report No. 87-03, 1987 (unpublished), p. 187.

[4] The Superconducting Super Collider Laboratory Report No. SSCL-SR-1185, 1992 (unpublished); K.Y. Ng, Fermilab Report No. FN-592, 1992 (unpublished).

[5] M. Syphers *et al.*, Phys. Rev. Lett. **71**, 719 (1993).

[6] J. Budnick, T. Hall, D. Li, and S.Y. Lee, in Proceedings of the IEEE Particle Accelerator Conference (IEEE, New York, in press).

[7] S.Y. Lee *et al.*, Phys. Rev. Lett. **67**, 3768 (1991); D.D. Caussyn *et al.*, Phys. Rev. A **46**, 7942 (1992).

[8] M. Ellison *et al.*, Phys. Rev. Lett. **70**, 591 (1993); H. Huang *et al.*, Phys. Rev. E **48**, 4678 (1993).

[9] The general steady-state solution can be expanded in multiples of the driving harmonics given by $g = \Sigma_n g_n \sin(n\omega_m t - \chi_n)$. The single-harmonic approximation of Eq. (2.7) is, however, a good approximation except at the modulation frequency near to the bifurcation frequency.

[10] *Handbook of Mathematical Functions*, Natl. Bur. Stand. Appl. Math. Ser. No. 55, edited by M. Abramowitz and I. A. Stegun (U.S. GPO, Washington, D.C., 1975).

[11] M.H.R. Donald and J.M. Paterson, IEEE Trans. Nucl. Sci. **NS26**, 3580 (1979); G.P. Jackson and R.H. Siemann, in *Proceeedings of IEEE Particle Accelerator Conference* (IEEE, New York, 1987), p. 1011; T. Ieiri and K. Hirata, in *ibid.* (IEEE, New York, 1989), p. 926.

[12] S. Smale, Bull. Am. Math. Soc. **73**, 747 (1967); J. Guckenheimer and P.J. Holmes, in *Nonlinear Oscillations, Dynamical Systems and Bifurcations of Vector Fields*, Applied Mathematical Sciences Vol. 42, edited by F. John, J. E. Marsden, and L. Strovich (Springer, Berlin, 1983); R.L. Kautz and J.C. Macfarlane, Phys. Rev. A **33**, 498 (1986); M. Bartuccelli *et al.*, Phys. Rev. B **33**, 4686 (1986); G. Cicogna, Phys. Lett. A **121**, 403 (1987). S.W. McDonald *et al.*, Physica D **17**, 125 (1985); B.P. Koch and R.W. Leven, *ibid.* **16**, 1 (1985).

[13] K.Y. Ng, Fermilab Report No. FN-604, 1993 (unpublished).

[14] G. Dôme, in CERN Report No. 87-03, 1987 (unpublished), p. 370; S. Krinsky and J.M. Wang, Part. Accel. **12**, 107 (1982).

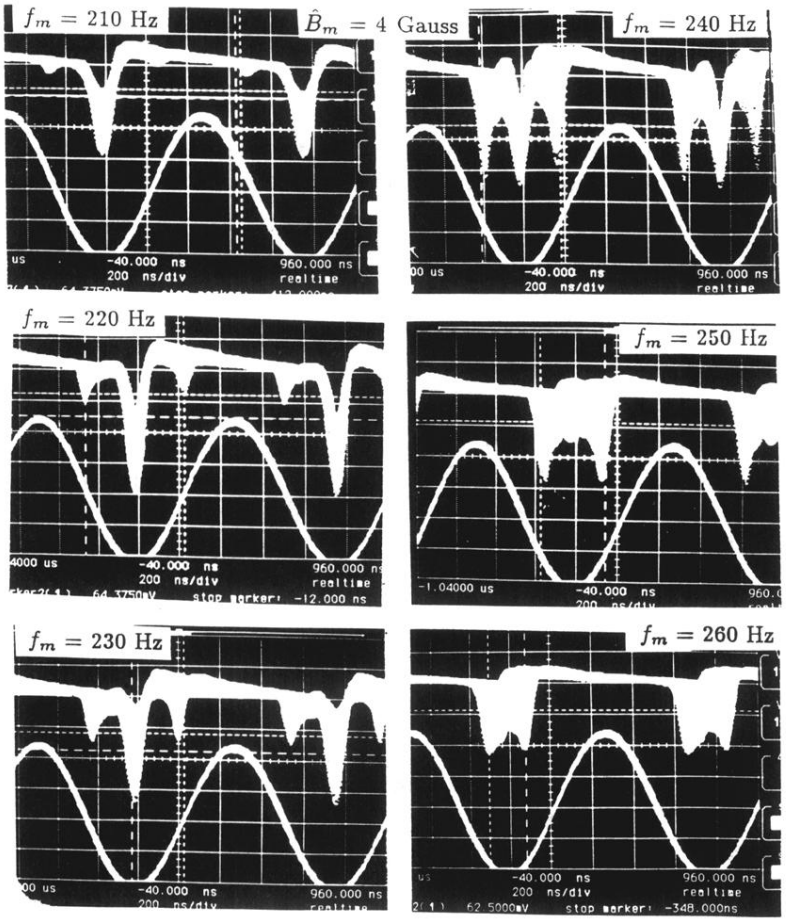

FIG. 2. The oscilloscope traces of accumulated BPM sum signals showed the splitting of beam bunch into beamlets below the bifurcation frequency. The modulation amplitude was $\hat{B}_m$ = 4 G. The sine waves in this figure were the rf wave form.

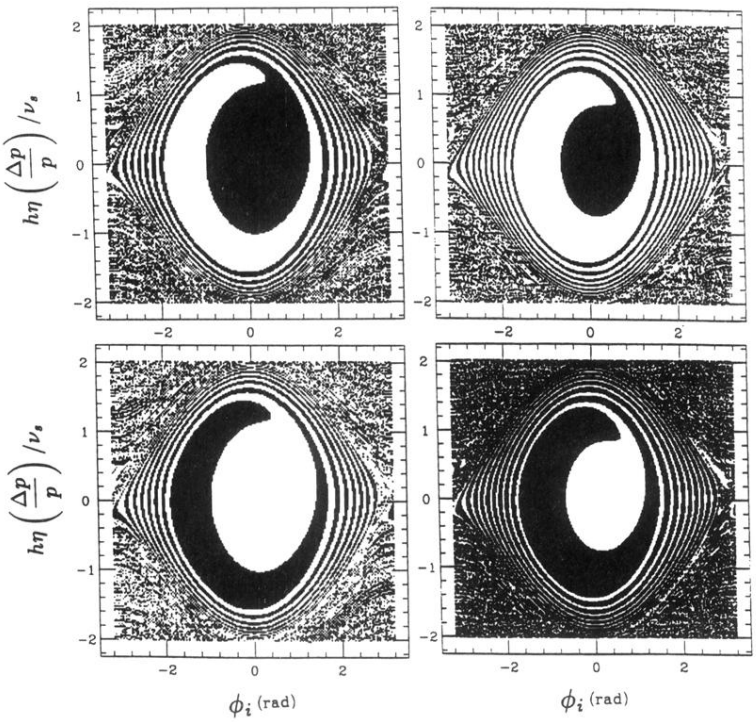

FIG. 7. The initial phase-space points, which damp to either the inner (upper graphs) or outer (lower graphs) attractors at modulation frequencies 230 Hz (left frames) and 240 Hz (right frames), obtained from numerical simulations are shown as black dots in phase space.